31st Annual International Conference of the IEEE EMBS
Minneapolis, Minnesota, USA, September 2-6, 2009

A Study on Using Texture Analysis Methods for Identifying Lobar Fissure Regions in Isotropic CT Images

Q. Wei, *Student Member, IEEE,* Y. Hu, *Member, IEEE*

***Abstract* – The major hurdle for segmenting lung lobes in computed tomographic (CT) images is to identify fissure regions, which encase lobar fissures. Accurate identification of these regions is difficult due to the variable shape and appearance of the fissures, along with the low contrast and high noise associated with CT images. This paper studies the effectiveness of two texture analysis methods – the gray level co-occurrence matrix (GLCM) and the gray level run length matrix (GLRLM) – in identifying fissure regions from isotropic CT image stacks. To classify GLCM and GLRLM texture features, we applied a feed-forward back-propagation neural network and achieved the best classification accuracy utilizing 16 quantized levels for computing the GLCM and GLRLM texture features and 64 neurons in the input/hidden layers of the neural network. Tested on isotropic CT image stacks of 24 patients with the pathologic lungs, we obtained accuracies of 86% and 87% for identifying fissure regions using the GLCM and GLRLM methods, respectively. These accuracies compare favorably with surgeons/radiologists' accuracy of 80% for identifying fissure regions in clinical settings. This shows promising potential for segmenting lung lobes using the GLCM and GLRLM methods.**

Keywords **– texture analysis, GLCM, GLRLM, lungs, lobar fissures, isotropic CT images.**

I. Introduction

LUNG cancer is the number one cause of cancer death in North America [1]. Its most effective treatment is lobectomy (surgical removal of diseased lung lobes). For preserving maximal lung function, this treatment depends on the precise assessment of the spatial relationships among cancer, lung lobes and other major anatomic structures. To perform this assessment, surgeons/radiologists routinely rely on reading two-dimensional (2D) clinical computed tomographic (CT) images (~ 3.0 mm in thickness). Reading clinical CT images is tedious, due to their single viewpoint and monotonic shades of gray, as shown in Fig. 1(a).

Using virtual reality technologies, three-dimensional (3D) visualization of lung cavities is becoming feasible for surgical planning of treating lung diseases [2]. Compared to 2D clinical CT images, 3D visualization offers unconstrained viewpoints, colors and no need of mental reconstruction, as illustrated in Fig. 1(b). Using manually segmented lung lobes, our recent study revealed that 3D visualization of lung cavities can significantly reduce surgeons' workload and planning time for surgical planning, as well as increase the accuracy of predicted lobectomy [3]. However, a challenge for this 3D visualization is the segmentation of lung lobes by identifying lobar fissures in 2D CT images.

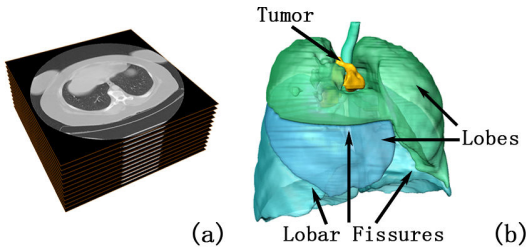

Fig. 1.Difference between the 2D view of clinical CT images (a) and 3D visualization of lung cavities reconstructed from a stack of 2D CT images by manually segmenting lung lobes (b).

To precisely localize lobar fissures, many research groups have used a two-stage approach: (1) find regions containing a fissure (i.e., fissure regions) in 2D CT images; and (2) refine the location and curvature of the fissure within the regions [4-7]. The precision of identifying fissure regions largely contributes to the final accuracy of segmenting the lung lobes. This identification is difficult due to the fissure's variable shape and appearance, along with the low contrast and high noise associated with both clinical and isotropic (~ 0.6 mm in thickness) CT images [8]. Often, this identification is complicated by various pathologies in the patients' lungs.

Nevertheless, there have been some efforts of identifying fissure regions. Wang et al. [4] developed an algorithm using manually segmented fissures to aid this identification. Zhang et al. [5] created an algorithm based upon a pulmonary atlas. However, this algorithm failed for some testing CT images of patients. Zhou et al. [6] and Ukil et al. [7] used the bronchial and vascular trees of the lung cavities to detect the fissure regions, respectively. Nevertheless, segmentation of these trees is time consuming and difficult to achieve [9]. Our preliminary work developed two algorithms for segmenting the lung lobes using a technique of adaptive fissure sweep to identify fissure regions [10, 11]. This technique worked well for the patients' lungs following a general lung anatomy, butfailed for lungs with abnormal anatomy or with severe pathologies. Thus, accurate identification of fissure regions remains an obstacle for precise segmentation of lung lobes.

In a CT image of cancerous lungs, there are four typical regions: fissure, air, bronchial and tumor. As shown in Fig. 2, a distinct texture characterizes each of these regions. These textures describe the spatial distribution of varying shades of gray and are easily identifiable by human eyes. Surgeons/radiologists normally rely on the subtle difference

Manuscript received March 30, 2009. This work was supported in part by the Natural Science and Engineering Research Council of Canada under Grant RGP312554-2008.

Q. Wei is with the Dept. of Electrical and Computer Engineering (ECE), University of Calgary (U of C), Calgary, AB, CANADA (e-mail: qwei@ucalgary.ca).

Y. Hu is with the Dept. of ECE, U of C, Calgary, AB, CANADA (phone: 403-220-4167; fax: 403-282-6855; e-mail: huy@ucalgary.ca).

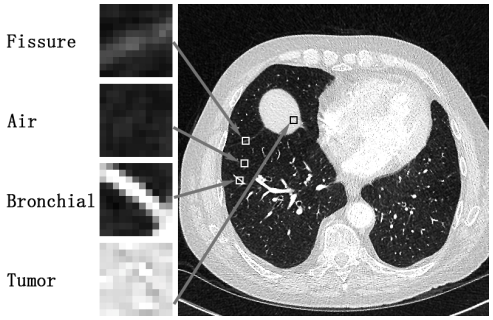

Fig. 2. An isotropic CT image of the human lungs showing the four types of regions: fissure, air, bronchial and tumor.

among these textures to identify fissure regions. It is therefore natural to apply texture analysis for computer-based identification of fissure regions. Even though many research groups pursued texture analysis on CT images for differentiating lung diseases [12], segmenting abdominal organs [13] and thrombotic tissue in the aorta [14], we could not find reports on using texture analysis for identifying fissure regions. To fill this vacuum, we conducted a study to examine the effectiveness of two common methods of texture analysis – the gray level co-occurrence matrix (GLCM) [15] and the gray level run length matrix (GLRLM) [16] – for identifying fissure regions among other types of regions in the human lungs (see Fig. 2). Because the computation of GLCM texture features differs from that of its GLRLM counterparts (refer to the Section II), it is difficult to theorize the suitability of each texture analysis method for identifying fissure regions. For this study, we are interested in achieving the highest accuracy of identifying fissure regions. Our goal is to investigate which of these methods is suitable for identifying fissure regions in CT images.

In this paper, we present our study with the following organization: Section II describes the methodology of the study. Section III presents study results, including a brief discussion. Section IV gives the conclusions and future work.

II. Methodology

We used isotropic CT image stacks of the lung cavities from 24 anonymous patients at the Foothills Medical Center, Calgary, Alberta. A Siemens Sensation 16 multi-slice CT scanner generated these image stacks with the same protocol and iodine contrast agent. Each image in a stack has an image resolution of 512 × 512 pixels with a thickness of 0.6 mm. For a patient with an average lung size, an image stack contains about 220 isotropic CT images. Of all patients, 22 had lung tumors. Using both GLCM and GLRLM methods, we classified all four regions within the human lungs as illustrated in Fig. 2 for our study. Fig. 3 gives the flowchart of classifying these four regions.

A. Filtering and Region Selection

Isotropic CT images are noisy compared to clinical CT counterparts [11]. To reduce noise, we applied the same Wiener filter as in our previous work [11]. For each CT image stack, we manually selected approximately 20 regions

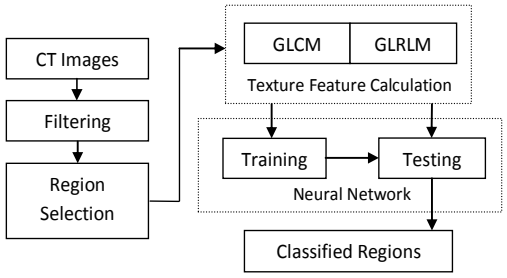

Fig. 3. Flowchart of evaluating the GLCM and GLRLM methods for classifying four typical regions in the human lungs.

of interest (ROIs) on every 5th slice of the stack, equivalent to clinical CT images with a thickness of 3.0 mm (each is compressed from 5 isotropic CT images). This selection resulted in roughly 880 ROIs for the isotropic CT image stack of a patient with an average lung size. Each ROI had a size of 10 × 10 pixels to approximate the width of fissure regions in isotropic CT images with a resolution of 512 × 512 pixels. For training a neural network, we predefined each ROI as one of the 4 regions: fissure, air, bronchial and tumor.

B. GLCM Texture Features

A GLCM is a 2D histogram, $P_{\theta,d}(i,j)$, describing how frequently two pixels with gray levels i, j occur jointly with an offset $[x\ y]$, where x and y are the horizontal and vertical distances between the two jointly occurring pixels.

For our study, we calculated a set of 32 GLCMs from each selected ROI described in Subsection A. This calculation is based upon 2 independent planes of a CT image stack (a 3D dataset) and 16 pairs of offset $[x\ y]$ on each plane. Given a CT image stack in the cross-sectional plane, we rotated the entire stack 90^0 clockwise and then re-sliced the rotated stack in the sagittal plane. This allowed us to analyze each ROI from both cross-sectional and sagittal planes. To identify fissure regions, we used 16 offsets ([0 1], [-1 1], [-1 0], [-1 -1], [-1 2], [-2 1], [-2 -1], [-1 -2], [-1 3], [-2 3], [-1 -3], [-2 -3], [-3 1], [-3 2], [-3 -1], [-3 -2]) instead of the original 4 offsets ([0 1], [-1 1], [-1 0], [-1 -1]) proposed by Haralick et al. [15]. We used these 16 offsets to capture a wide range of fissure orientations. For each of the 32 GLCMs, we calculated all 14 texture features proposed by Haralick et al. [15]. This results in a total of 448 texture features for a single ROI. We used all of them for the purpose of achieving the highest accuracy of identifying fissure regions. This number of texture features could be later optimized to reduce computation time.

The computation of each GLCM requires the scaling of gray-level pixel intensity within the ROIs into certain quantized levels. However, no guidelines exist for selecting proper quantized levels [17]. The ideal number of quantized levels, Q, is highly dependent on tissue textures. To find the ideal Q for identifying fissure regions, we varied the number of quantized levels Q from 8 to 64, in 2^q increments (q = 3, 4, 5, 6). This range of quantized levels balances between the scaling of gray-level pixel intensity and computation time.

C. GLRLM Texture Features

Unlike a GLCM which stores the probability of two gray

levels occurring at a predefined radius and direction, a GLRLM is a 2D histogram, $R_\theta(i,j)$, recording the number of run length primitives with gray level i and run length j in the direction θ [16]. A run length primitive is a maximum set of same gray-level pixels connected in a line.

For identifying fissure regions, we used the same 2 planes and 16 offsets for calculating the GLRLMs as we did for computing the GLCMs. This resulted in 32 GLRLMs for a single ROI. On the basis of 11 texture features proposed by Galloway [16], we computed a total of 352 texture features for each ROI. We used all of these features for obtaining the highest accuracy of identifying fissure regions. Same as with the GLCMs, we varied the number of quantized levels Q from 8 to 64, in 2^q increments (q = 3, 4, 5, 6).

D. Neural Network

To evaluate the performance of both GLCM and GLRLM texture features for identifying fissure regions, we applied a neural network (NN) to classify the ROIs selected in the Subsection A. For simplicity and flexibility, we used a 3 layer feed-forward back-propagation NN [18]. We utilized supervised training for this NN to learn the patterns associated with various inputs by fitting a parametric model over them. Once trained, the NN can then classify unknown patterns based on what it has learned.

For this NN, we used a linear function for the output layer and a Log-Sigmoid transfer function for both input and hidden layers [18]. The output layer contains 4 neurons, corresponding respectively to four types of regions in the human lungs (see Fig. 2). The selection of the ideal number of neurons for the input and hidden layers (input/hidden layers) is a non-trivial task and often based on trial-and-error. We investigated the effects of neuron numbers in the input/hidden layers (both have the same number of neurons) on classifying the ROIs. The number of neurons N varied from 4 to 128 in 2^n increments (n = 2, 3, 4, 5, 6, 7). For the classification, we applied the following procedure:

1. Compute the GLCM and GLRLM texture features for all ROIs in the CT image stacks of 24 patients.
2. Select randomly 5 of 24 image stakes as training data.
3. Train the NN using either the GLCM or GLRLM texture features from the training data in Step 2. The predefined ROIs described in Subsection A serve as the targets for this supervised training.
4. Classify all ROIs from the remaining 19 image stacks.
5. Repeat 10 times from Step 2 to Step 4 to average out the randomness of initializing the NN's weights and selecting training data.

To find the optimal quantized level Q and the number of neurons N, we repeated the above procedure for Q from 8 to 64, in 2^q increments (q = 3, 4, 5, 6) and for N from 4 to 128, in 2^n increments (n =2, 3, 4, 5, 6, 7).

III. Results and Discussions

Using a 3.2 GHz Xeon Duo computer with 2 GB RAM running Matlab 7.0.4 (R14), we performed classification of the four regions in the human lungs: fissure, air, bronchial, and tumor regions for all 24 isotropic CT image stacks (about 880 ROIs/stack). We compared the resulting classification from the NN to our predefined targets. We utilized true positive (*TP*), true negative (*TN*), false positive (*FP*) and false negative (*FN*) to measure the performance of the classification. We also calculated the sensitivity, specificity, and accuracy of the classification by:

$$sensitivity = \frac{TP}{TP + FN}\ , \tag{1}$$

$$specificity = \frac{TN}{TN + FP}, and \tag{2}$$

$$accuracy = \frac{TP + TN}{TP + FP + TN + FN}. \tag{3}$$

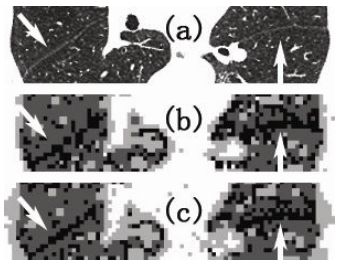

Fig. 4. Examples of classification: (a) original CT image; (b) classified image using the GLCM method; and (c) classified image using the GLRLM method. The pixels in black, dark gray and light gray represent classified fissure, air and bronchial regions, respectively. White arrows indicate fissures and identified fissure regions. [These examples are fissure regions cropped from the CT images due to limited space here].

Fig. 4 illustrates examples of classifying an isotropic CT image without tumor using the GLCM texture features (the GLCM method) and its GLRLM counterparts (the GLRLM method). Both methods produced very distinguishable fissure regions, as highlighted by white arrows. This reveals that both methods of texture analysis are able to identify fissure regions. In addition, both methods yielded similar results in classifying air and bronchial regions.

Fig. 5 shows a surface plot of the average accuracy for classifying the four types of regions in the human lungs using the GLCM method. For this plot, we used the quantized levels, Q = 8, 16, 32, 64, and the number of neurons in the input/hidden layers, N = 4, 8, 16, 32, 64, 128. As shown in Fig. 5, the average accuracy of the classification decreases dramatically for Q > 16. In contrast, the accuracy remains fairly stable no matter the number of neurons in the input/hidden layers. The highest overall accuracy of 90% occurred with Q = 16 and N = 64.

Fig. 6 illustrates a surface plot of the average accuracy for the classification using the GLRLM method with the same quantized levels and number of neurons as in Fig 5. Unlike the accuracy of the GLCM method, the accuracy of the GLRLM method is fairly constant for different quantized levels. However, the accuracy of the GLRLM method is highly dependent on the number of neurons in the input/hidden layers. As shown in Fig. 6, the highest overall accuracy of the GLRLM method reached 91% with Q = 16 and N = 32. The GLRLM method attained an overall accuracy of 90% with Q = 16 and N = 64.

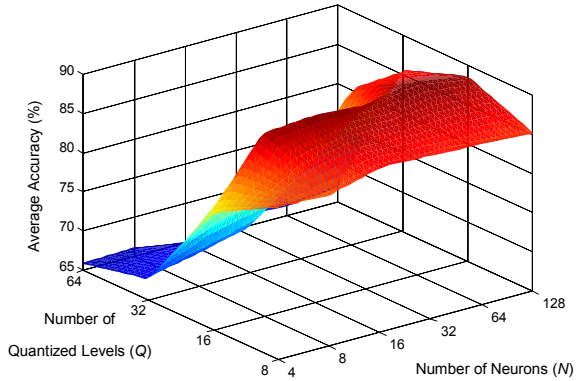

Fig. 5. Surface plot of the average classification accuracy for the four types of regions in the human lungs using the GLCM method.

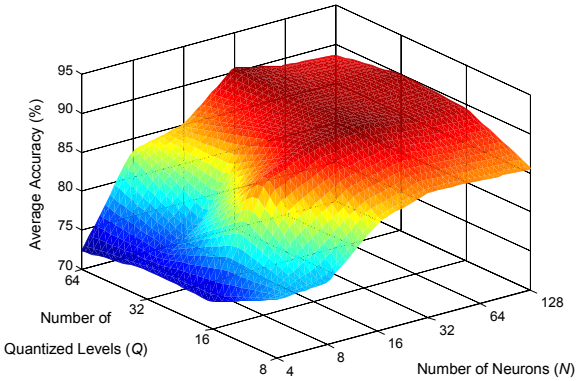

Fig. 6. Surface plot of the average classification accuracy for the four types of regions in the human lungs using the GLRLM method.

Using both GLCM and GLRLM methods with $Q = 16$ and $N = 64$, Table I shows the sensitivity, specificity and individual accuracy of classifying the 4 types of regions in the lungs. The sensitivities of the GLCM method were notably lower than those of the GLRLM method for air and tumor regions. Both methods yielded comparable sensitivities for the rest of regions. Both methods achieved similar specificities for all types of regions, although the GLCM method gave slightly lower accuracy than the GLRLM method. For fissure regions in particular, both methods had an accuracy of 86% and 87%, respectively. This compares favorably with the accuracy of 80% for surgeons/radiologists identifying fissure regions in clinical CT image stacks [10]. Without optimization, average computation time for the GLCM texture features is about 25% longer than that for the GLRLM counterparts, as shown in Table I. Considering both classification accuracy and computation time, the GLRLM method is better suited for identifying fissure regions.

TABLE I
CLASSIFICATION OF FISSURE, AIR, BRONCHIAL AND TUMOR REGIONS

		Regions				Avg. Time (s)
		Fissure	Air	Bronchial	Tumor	
GLCM (%)	Sensitivity	82	77	91	64	105
	Specificity	90	92	92	98	
	Accuracy	88	88	92	92	
GLRLM (%)	Sensitivity	79	80	92	68	75
	Specificity	91	91	93	98	
	Accuracy	87	88	93	93	

IV. CONCLUSION AND FUTURE WORK

We studied the effectiveness of using the GLCM and GLRLM methods for identifying fissure regions by classifying the four types of regions in the human lungs. We obtained the best accuracy for identifying all these regions using a feed-forward back-propagation NN, with 16 quantized levels and 64 neurons. Although both methods yielded similar accuracies, the GLRLM method required less computation time. This makes the GLRLM method a better candidate for identifying fissure regions. Future work includes reducing the number of texture features, optimizing the computation of the GLRLM method and combining it with our wavelet algorithm [11] to detect fissures for segmenting lung lobes.

REFERENCES

[1] American Cancer Society, "Cancer Facts & Figures," [Online], 2008, Available at: http://www.cancer.org/docroot/STT/stt_0.asp

[2] B. M. Hemminger, P. L. Molina, T. M. Egan, F. c. Detterbeck, K. E. Muller, C. S. Coffrey, and J. K. Lee, "Assessment of real-time 3D visualization for cardiothoracic diagnostic evaluation and surgery planning," *J. Digital Imag.*, vol. 18, pp. 145-153, 2005.

[3] Y. Hu and R. A. Malthaner, "The feasibility of three-dimensional displays of the thorax for preoperative planning in the surgical treatment of lung cancer," *Europ. J. Cardio-Thoracic Surg.*, vol. 31, pp. 506-511, 2007.

[4] J. Wang, M. Betke, and J. P. Ko, "Pulmonary fissure segmentation on CT", *Med. Image Anal.*, vol. 10, pp. 530-547, 2006.

[5] L. Zhang, "Atlas-Driven Lung Lobe Segmentation in volumetric X-Ray CT images," *Ph.D. thesis*, Univ. Iowa, Iowa City, Dec. 2002.

[6] X. Zhou, T. Hayashi, T. Hara, H. Fujita, R. Yokoyama, T. Kiryu, and H. Hoshi, "Automatic segmentation and recognition of anatomical lung structures from high-resolution chest ct images," *Compu. Med. Imag. Graphics*, vol. 30, pp. 299-313, 2006.

[7] S. Ukil and J.-M. Reinhardt, "Anatomy-Guided Lung Lobe Segmentation in X-Ray CT Images," *IEEE Trans. Med. Imag.*, vol. 28, pp. 202-214, 2009.

[8] W. R. Webb, N. L. Muller, and D. P. Naidich, *High-resolution CT of the Lung,* 3rd ed., Philadelphia, PA: Lippincott, Williams and Wilkins, 2001.

[9] J. Tschirren, E. A. Hoffman, G. McLennan, and M. Sonka, "Intrathoracic airway trees: segmentation and airway morphology analysis from low-dose CT scans," *IEEE Trans. Med. Imag.,* vol. 24, pp. 1529-1539, 2005.

[10] Q. Wei, Y. Hu, J. H. Macgregor, and G. Gelfand, "Segmentation of lung lobes in clinical CT images," *Int. J. CARS,* vol. 3, pp. 151-163, 2008.

[11] Q. Wei, Y. Hu, G. Gelfand, and J. H. Macgregor, "Segmentation of lung lobes in high-resolution isotropic CT images," *IEEE Trans. Biomed. Eng.*, vol. 56, pp. 1383-1393, 2009.

[12] F. Chabat, G.-Z. Yang, and D. M. Hansell, "Obstructive lung diseases: texture classification for differentiation at CT," *Radiology*, vol. 228, pp. 871-877, 2003.

[13] L. Tesar, A. Shimizu, D. Smutek, H. Kobatake, and S. Nawano, "Medical image analysis of 3D CT images based on extension of Haralick texture features," *Comput. Med. Imag. and Graphics*, vol. 32, pp. 512-520, 2008.

[14] B. Podda, A. Giachetti, "Texture analysis of CT images for vascular segmentation: a revised run length approach," *ICIAP*, 2005.

[15] R. M. Haralick, K. Shanmugan, and I. Dinstein, "Textural features for image classification," *IEEE Trans.* Sys., *Man and Cybern., vol. SMC-3*, pp. 610-621, November 1973.

[16] M. Galloway, "Texture analysis using gray level run lengths," *Comput. Graphics Image Proc.*, vol. 4, pp. 172-199, 1974.

[17] A. Giachetti, "Improving feature extraction methods for CT texture analysis," *Proc. 9th IASTED Intl. Conf.*, Innsbruck, Austria, 2007.

[18] J. A. Anderson, *An Introduction to Neural Networks*. Cambridge, MA: MIT Press, 1995.